Nonreciprocal Magnetoacoustic Waves in Dipolar-Coupled Ferromagnetic Bilayers

M. Küß[1,*] M. Heigl,[2] L. Flacke,[3,4] A. Hörner,[1] M. Weiler,[3,4,5] A. Wixforth,[1] and M. Albrecht[2]

[1]*Experimental Physics I, Institut of Physics, University of Augsburg, Augsburg 86135, Germany*

[2]*Experimental Physics IV, Institut of Physics, University of Augsburg, Augsburg 86135, Germany*

[3]*Walther-Meißner-Institut, Bayerische Akademie der Wissenschaften, Garching 85748, Germany*

[4]*Physics Department, Technical University Munich, Garching 85748, Germany*

[5]*Fachbereich Physik and Landesforschungszentrum OPTIMAS, Technische Universität Kaiserslautern, Kaiserslautern 67663, Germany*

We study the interaction of surface acoustic waves (SAWs) with spin waves (SWs) in a $Co_{40}Fe_{40}B_{20}/Au/Ni_{81}Fe_{19}$ system composed of two ferromagnetic layers separated by a nonmagnetic Au spacer layer. Because of interlayer magnetic dipolar coupling between the two ferromagnetic layers, a symmetric and an antisymmetric SW mode form, which both show a highly nondegenerate dispersion relation for oppositely propagating SWs. Due to magnetoacoustic SAW-SW interaction, we observe highly nonreciprocal SAW transmission in the piezoelectric-ferromagnetic hybrid device. We experimentally and theoretically characterize the magnetoacoustic wave propagation as a function of frequency, wave vector, and external magnetic field magnitude and orientation. Additionally, we demonstrate that the nonreciprocal SW dispersion of a coupled magnetic bilayer is highly tuneable and not limited to ultrathin magnetic films, in contrast to the nonreciprocity induced by the interfacial Dzyaloshinskii-Moriya interaction. Therefore, magnetoacoustic coupling in ferromagnetic multilayers provides a promising route towards building efficient acoustic isolators.

I. INTRODUCTION

Microwave isolators have found wide applications in a variety of devices for signal processing. However, for on-chip devices, miniaturization remains an important challenge. Microwave isolators rely on nonreciprocity, which means that the signal propagation is not symmetric under inversion of the propagation direction [1]. Nonreciprocity requires breaking of time-reversal symmetry [2,3]. Because time-reversal symmetry is a fundamental law of mechanics [4,5], nonreciprocity is a rarely observed phenomenon.

Surface acoustic waves (SAWs) are used in many everyday devices as the basis for miniaturized filters and delay lines due to the greatly reduced wavelength of SAWs compared to free-space microwaves of the same frequency. However, SAWs in general propagate reciprocally. Motivated by the benefits that SAW technology offers, such as mass fabrication capabilities and small device geometry, multiple mechanisms breaking the reciprocity of SAW propagation have so far been investigated. This can be achieved, for instance, by coupling SAWs with two-dimensional electron systems [6,7].

Moreover, coupling SAWs with spin waves (SWs) in magnetic media is a straightforward approach to obtain nonreciprocity. In this case the SAW-SW coupling mechanism itself is already nonreciprocal, because of a helicity mismatch between the SAW-induced magnetoacoustic driving fields and the fixed chirality of the magnetization precession [8–14]. Furthermore, the SW dispersion relation can be nonreciprocal. For instance, the Dzyaloshinskii-Moriya interaction (DMI) induces SW nonreciprocity [15–17] and therefore nonreciprocal SAW propagation, as recently theoretically [18] and experimentally demonstrated for ultrathin ferromagnetic/heavy metal bilayers [12]. In addition, it was shown many years ago that the SW dispersion can be highly nonreciprocal in magnetic multilayers [19–21], which was very recently exploited to obtain nonreciprocal SAW transmission in a Fe-Ga-B/Al_2O_3/Fe-Ga-B magnetic bilayer system for frequencies up to 1.4 GHz [22].

Here, we experimentally demonstrate the interaction of SAWs and SWs in a magnetoacoustic hybrid device to obtain highly nonreciprocal magnetoacoustic surface waves (MASWs) for frequencies up to 7.0

*matthias.kuess@physik.uni-augsburg.de

GHz. We show that nonreciprocal symmetric and anti-symmetric SW modes form in a magnetically dipolar-coupled $Ni_{81}Fe_{19}/Au/Co_{40}Fe_{40}B_{20}$ (Py/Au/CoFeB) layer system. In combination with the amplitude nonreciprocity caused by the SAW-SW helicity mismatch effect, double-nonreciprocal MASWs arise. We model our results in a phenomenological approach and discuss the high tuneability of the nonreciprocity by, for example, increasing the film thicknesses and changing the saturation magnetization of the magnetic layers. Due to the tunability, this approach has promising prospects as a basis for miniaturized microwave acoustic isolators.

The magnetoacoustic hybrid device, investigated in this study, is schematically depicted in Fig. 1. A SAW is launched on the piezoelectric $LiNbO_3$ substrate by applying an alternating voltage signal with the resonance frequency of the interdigital transducer (IDT). This strain wave propagates through the magnetic film and potentially couples with SWs because of magnetoelastic [8,23,24], magneto-rotation [11,12,25], spin-rotation [26–28], and gyromagnetic coupling [29]. Note that in this study, we consider magnetoelastic and magneto-rotation coupling. This is sufficient to describe our experimental results very well. Magneto-rotation coupling arises since the rotational lattice motion of the SAW causes reorientation of the surface-normal direction, which couples via the magnetic anisotropy fields and the dipolar shape anisotropy to the magnetization [11]. The nonreciprocity of the excited MASW is characterized by inverting its propagation direction, respectively its wave vector k_{Sij} with $ij \in \{21, 12\}$.

For a thin magnetic single layer, a typical reciprocal SW dispersion in the Damon-Eshbach configuration ($\phi_0 \approx 90°$) is shown in Fig. 2(a). The dispersion of the SAW is linear with $\omega = 2\pi f = c_{SAW}|k|$ and depends on its phase
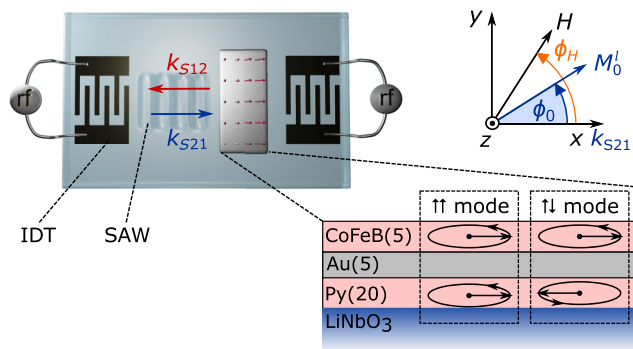

FIG. 1. Illustration of the investigated magnetoacoustic hybrid device and the coordinate system used. The nonreciprocity of the MASW in the magnetic bilayer Py(20 nm)/Au(5 nm)/CoFeB (5 nm) is characterized by different transmission magnitudes of oppositely propagating waves k_{S21} and k_{S12}. A symmetric (↑↑) and an antisymmetric (↑↓) SW mode can be excited in the magnetic bilayer. This is schematically shown by the trajectory of the precessing magnetic moments (black arrows).
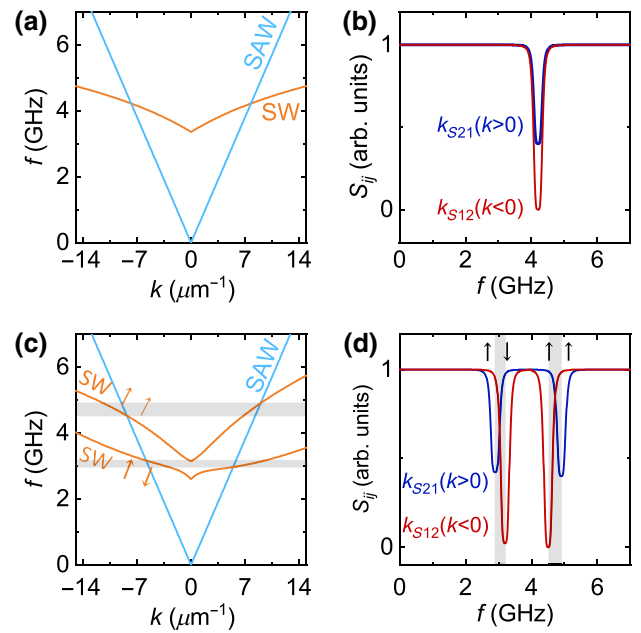

FIG. 2. Illustration of the nonreciprocity (a),(b) in a magnetic single layer and (c),(d) in a dipolar-coupled magnetic bilayer for $\phi_0 = 89°$. Whereas the SW dispersion relation of the single layer (a) is reciprocal, the SW dispersion relation of the bilayer (c) is nonreciprocal (highlighted by shaded areas) and is composed of a high-frequency symmetric mode (↑↑) and a low-frequency antisymmetric mode (↑↓). MASWs form in the vicinity of the SAW-SW dispersion intersection points, which are experimentally observed by a decrease in the SAW transmission S_{ij} (b),(d). Additionally, the SAW-SW helicity mismatch effect is present in both samples and induces different transmission magnitudes $S_{21} \neq S_{12}$ at resonance.

velocity c_{SAW} and its frequency f. In proximity to the intersection of SAW and SW dispersion, the SAW can excite SW dynamics and a MASW forms. As a result, the amplitude of the SAW transmission S_{ij} decreases [8] as schematically depicted in Fig. 2(b). The SAW transmission at resonance potentially differs for oppositely propagating waves. This is a consequence of the nonreciprocal SAW-SW helicity mismatch effect [8–10].

A typical SW dispersion of an asymmetric magnetic bilayer separated by a nonmagnetic spacer layer is shown in Fig. 2(c). By decreasing the spacer layer thickness, the two uncoupled reciprocal Damon-Eshbach SW modes of both thin magnetic layers become coupled via the dipolar stray fields of the SWs. Thus, two branches form, which correspond to symmetric (in-phase) and antisymmetric (out-of-phase) modes [30,31], as schematically illustrated in Fig. 1. Note that for very thin spacer layers, inter-layer exchange interaction must be considered additionally [32,33]. Since the dipolar energy of both modes differs and depends on the SW propagation direction k_{ij}, both modes are nondegenerate and nonreciprocal [34]. Consequently,

two dips with shifted nonreciprocal resonance frequencies are expected in the SAW transmission, as shown in Fig. 2(d). Together with the amplitude nonreciprocity, being caused by the SAW-SW helicity mismatch effect, this results in double-nonreciprocal SAW transmission with a high nonreciprocity contrast.

II. THEORY

The complete theoretical approach, including the calculation of the SW dispersion, based on Ref. [34], can be found in the Supplemental Material [35]. For simplicity, we here assume for both magnetic layers $l \in \{A, B\}$ (i) parallel alignment of the static in-plane magnetizations $\mathbf{M}_0^l = M_s^l \mathbf{m}$ with the saturation magnetizations M_s^l and (ii) identical displacement fields, which are induced by the SAW. The direction of the magnetizations $\mathbf{m}$ can be adjusted by an external field $\mathbf{H}$ and encloses the angle $\phi_0 = \phi_0^A = \phi_0^B$ with the x axis of the Cartesian coordinate system (see Fig. 1). Additionally, we use rotated 123-coordinate systems to calculate the magnetization dynamics [8], where the 3 axis is parallel to $\mathbf{M}_0^l$ and the 2 axis (1 axis) is aligned in (perpendicular to) the xy plane.

In the dipolar-coupled magnetic bilayer, the SAW induces displacement fields u_i, strain $\epsilon_{ij} = \frac{1}{2}(\partial u_i/\partial j + \partial u_j/\partial i)$, and lattice rotation $\omega_{ij} = \frac{1}{2}(\partial u_i/\partial j - \partial u_j/\partial i)$ with $i, j \in \{x, y, z\}$. For the Rayleigh-type SAW, the nonzero complex amplitudes of ϵ_{ij} and ω_{ij} are $\epsilon_{xx,0}, \epsilon_{zz,0}, \epsilon_{xz,0}$, and $\omega_{xz,0}$, respectively [11,12]. These give rise to magnetoelastic and magneto-rotation SAW-SW coupling and induce driving fields with complex amplitudes

$$\mathbf{h}^l = \frac{2}{\mu_0} \cos(\phi_0) \begin{pmatrix} b_{2,\text{eff}}^l \epsilon_{xz,0} \\ b_1^l \epsilon_{xx,0} \sin(\phi_0) \end{pmatrix} \quad (1)$$

in the 12 plane. Here b_1^l are the isotropic magnetoelastic coupling constants for polycrystalline films. Additionally, $b_{2,\text{eff}}^l$ are vertical effective coupling constants that consider magnetoelastic and magneto-rotation coupling and depend on $\omega_{xz,0}$ [35]. The magnetoacoustic driving fields potentially induce elliptical magnetization precession around the equilibrium magnetization direction $\mathbf{M}_0^l$ with complex amplitudes $\mathbf{M}_{12}^l = (M_1^l, M_2^l)$ in the 12 plane, as shown in Fig. 1. Similar to a single layer [8], the absorbed power of the SAW in the magnetic bilayer is

$$P_{\text{abs}} = \frac{\omega \mu_0}{2} \sum_l V^l \text{Im}\left\{\mathbf{h}^{l*} \cdot \mathbf{M}_{12}^l\right\} \quad (2)$$

in the limit of small film volumes V^l.

Due to large interlayer dipolar coupling, both symmetric and antisymmetric SW modes arise. The mode shape determines the SW excitation efficiency of the SAW. Thus,

we calculate P_{abs} with Eqs. (1) and (2) and obtain

$$\begin{aligned} P_{\text{abs}}^{\pm} = \omega \cos \phi_0 \text{Im}\Big\{ & \epsilon_{xz,0}^* \left[V^B b_{2,\text{eff}}^B M_1^B \pm V^A b_{2,\text{eff}}^A M_1^A \right] \\ & + \epsilon_{xx,0}^* \sin \phi_0 \left[V^B b_1^B M_2^B \pm V^A b_1^A M_2^A \right] \Big\}, \end{aligned} \quad (3)$$

where the $+$ sign corresponds to the symmetric mode and the $-$ sign to the antisymmetric mode. The absorbed SAW power differs for the symmetric and antisymmetric mode and depends on the sign of the coupling constants $b_{2,\text{eff}}^l$, b_1^l, on the ratio of the magnetic thin-film volumes, and on the precession amplitudes $M_{1,2}^l$. For identical films A and B, it is not possible to excite the antisymmetric SW mode and we obtain $P_{\text{abs}}^- = 0$. In contrast, for films with inverted signs for the coupling constants (e.g. CoFeB, Ni) the symmetric SW mode is suppressed.

Furthermore, the nonreciprocity that is caused by the SAW-SW helicity mismatch effect can be tuned by adjusting the properties of both ferromagnetic layers. For the Rayleigh wave, the strain $\epsilon_{xz,0}$ is phase-shifted by $90°$ with respect to $\epsilon_{xx,0}$ [8]. If the propagation direction of the SAW is inverted, the strain $\epsilon_{xz,0}$ changes sign (with respect to $\epsilon_{xx,0}$) and the helicities of the driving fields $\mathbf{h}^l$ are inverted. This results, together with the favored, right-handed rotational sense of the magnetization precession, in a nonreciprocal excitation efficiency that has so far only been studied in magnetic single layers [8–14].

In magnetic bilayers, the amplitude nonreciprocity is additionally modulated by the symmetry of the SW mode. This can be recognized by inspection of the term proportional to $\epsilon_{xz,0}^*$ given in Eq. (3). Since the magnitude of this term depends on the symmetry of the SW mode, the latter also modulates the amplitude nonreciprocity.

III. EXPERIMENTAL METHODS

We use dc magnetron sputterdeposition to prepare one sample with a dipolar-coupled magnetic bilayer Py(20)/Au(5)/CoFeB(5) (numbers are the nominal thicknesses in nanometers) and two samples with magnetic single layers Py(20)/Au(5) and CoFeB(5)/Pt(3). The compositions of the Py and CoFeB sputter targets are permalloy ($Ni_{81}Fe_{19}$) and $Co_{40}Fe_{40}B_{20}$, respectively. All samples are covered with an additional $Si_3N_4(3)$ layer to protect the samples from oxidation. More details about the sample geometry and preparation of samples with the IDTs are given in the Supplemental Material [35]. The CoFeB(5)/Pt(3) sample, exhibiting DMI, is identical to one of the samples used in Ref. [12].

First, we carry out superconducting quantum interference device-vibrating sample magnetometry (SQUID-VSM) measurements to determine the saturation magnetization M_s of all samples. Second, we perform broadband ferromagnetic resonance (FMR) measurements to obtain values for the g factor, the effective magnetization M_{eff}, and

the effective damping constant $\alpha_{\text{eff}}^{\text{FMR}} = \mu_0 \Delta H \gamma / (2\omega) + \alpha^{\text{FMR}}$ [12], which includes Gilbert damping α^{FMR} and inhomogeneous line broadening ΔH. The uniform excitation mode, which is excited in FMR measurements, does not show any static [32,33] or dynamic [36,37] interlayer exchange coupling between the individual magnetic layers of the Py(20)/Au(5)/CoFeB(5) sample, because of the relatively thick spacer layer. Thus, we attribute the observed interlayer coupling in our experiments solely to the dipolar magnetic stray fields of the SWs.

The SAW transmission of our delay lines is measured with a vector network analyzer. Based on the low propagation velocity of the SAW, a time-domain gating technique is employed to exclude spurious signals [38], in particular electromagnetic crosstalk. This enables us to study SWs with frequencies up to $f = 7.0$ GHz. We use the relative change of the background-corrected SAW transmission signal as $\Delta S_{ij} (\mu_0 H) = S_{ij} (\mu_0 H) - S_{ij} (-200\,\text{mT})$ to characterize SAW-SW coupling. Here ΔS_{ij} is the magnitude of the complex transmission signal with $ij \in \{21, 12\}$.

IV. RESULTS AND DISCUSSION

In Fig. 3, we study the SAW transmission ΔS_{ij} as a function of the external magnetic field magnitude H and direction ϕ_H. The experimental results for the CoFeB(5)/Pt(3)

magnetic single layer are shown in Fig. 3(a). As discussed in Ref. [12], the fourfold symmetry in ΔS_{ij} reflects the main symmetry of the magnetoacoustic driving field $\mathbf{h}_{\text{CoFeB}}$ in Eq. (1). Since the longitudinal strain is much higher than the vertical shear strain ($|\epsilon_{xx,0}| \gg |\epsilon_{xz,0}|$) and the coupling constants $b_1^{\text{CoFeB}}, b_{2,\text{eff}}^{\text{CoFeB}}$ are comparable, the main magnetoacoustic driving field component is aligned in plane with a fourfold symmetry $\propto \sin\phi_0 \cos\phi_0$ [24]. Due to the SAW-SW helicity mismatch effect this fourfold symmetry is broken and gives rise to an amplitude nonreciprocity for the resonant fields [12]. Furthermore, the resonance fields are nonreciprocally shifted because of DMI [12].

For a perfect $\text{Ni}_{81}\text{Fe}_{19}$ thin film, the saturation magnetostriction is expected to vanish [40]. Therefore, for purely magnetoelastic coupling, we expect a vanishing magnetoacoustic response for the Py single layer, which is in contrast to the experimental results shown in Fig. 3(b). Besides magnetoelastic coupling, various other SAW-SW coupling mechanisms have been reported in the literature, such as spin-rotation coupling [26–28], magneto-rotation coupling [11,12,25], and gyromagnetic coupling [29]. As all these effects induce driving fields with a symmetry $\propto \cos\phi_0$, it is difficult to distinguish between them. This was already noted by Xu *et al.* for spin- and magneto-rotation coupling [11]. Because we cannot differentiate
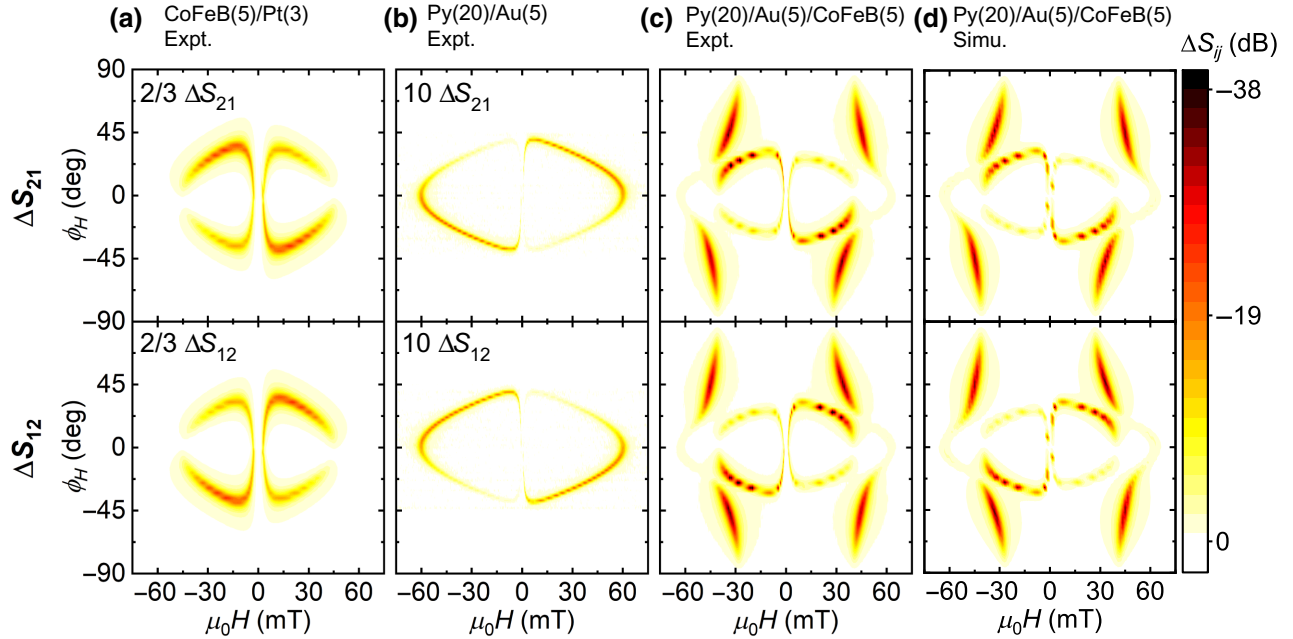

FIG. 3.   Change of the SAW transmission ΔS_{21} (upper row) and ΔS_{12} (lower row) of (a) a CoFeB(5)/Pt(3) [12] magnetic single-layer sample, (b) a Py(20)/Au(5) magnetic single-layer sample, and (c) a Py(20)/Au(5)/CoFeB(5) magnetic bilayer sample as a function of orientation and magnitude of the external magnetic field at 6.77, 6.86, and 6.87 GHz. The numbers in parentheses are the nominal film thicknesses in nanometers. To compensate for the greater length of the CoFeB(5)/Pt(3) film (750 μm instead of 500 μm), the response of the CoFeB(5)/Pt(3) film is scaled by 2/3 [39]. The low response of Py(20)/Au(5) is multiplied by a factor of ten. (d) Simulated response of the magnetic bilayer. The discrete appearance of the low-field resonance in (c),(d) is an artifact, which is caused by the incremental step size of $\phi_H = 3.6°$.

between the three coupling mechanisms, we solely consider magnetoelastic and magneto-rotation coupling in our modeling, which is sufficient to describe our experimental results. In the Supplemental Material [35] we show the excellent agreement between experiment and curve fitting results for the CoFeB and Py magnetic single layers [12]. Nevertheless, it might be possible that all of these mechanisms contribute at the same time to the magnetoacoustic response in Fig. 3.

We attribute the experimental findings for the Py(20)/Au(5) film to the following effects. First, ΔS_{ij} is about ten times lower compared to the CoFeB single layer and does not show a fourfold symmetry, which is caused by the small magnetoelastic coupling. The main contribution of the driving field has a symmetry $\propto \cos\phi_0$ and therefore is caused by magneto-rotation coupling and proportional to $b_{2,\mathrm{eff}}^{\mathrm{Py}}$. Because the Py sample also shows a pronounced amplitude nonreciprocity, the magnetoelastic driving fields with the symmetry $\propto b_1^{\mathrm{Py}} \sin\phi_0 \cos\phi_0$ are small, but not zero. The nonreciprocity, induced by the SAW-SW helicity mismatch effect, is inverted for both single-layer samples, due to an opposite sign of b_1^{Py} and b_1^{CoFeB}.

The experimental results for the dipolar-coupled magnetic bilayer are shown in Fig. 3(c). Because of large interlayer dipolar coupling, two resonances form, which can be related to symmetric and antisymmetric SW modes. Additionally, the positions of the resonance fields are nonreciprocal due to the nonreciprocity of the SW dispersion relation. The main symmetry of ΔS_{ij} follows the fourfold symmetry of the dominating driving field component, which originates from the CoFeB layer. Interestingly, the low-field resonance shows a high degree of amplitude nonreciprocity, whereas the amplitude nonreciprocity of the high-field resonance is low.

We quantitatively simulate the response of the magnetic bilayer in Fig. 3(d). Our modeling is based on the analytical Landau-Lifshitz-Gilbert approach of Ref. [8], but in addition takes into account an exponentially decaying amplitude of the SAW along the SAW propagation direction [12]. Effective fields caused by the (i) Zeeman energy, (ii) in-plane uniaxial magnetic anisotropy, (iii) out-of-plane surface anisotropy, (iv) intralayer exchange interaction, (v) intralayer dipolar fields of the SW, and (vi) magnetoacoustic driving fields of Eq. (1) are considered for both layers [12]. Furthermore, the interlayer dipolar coupling is mediated by effective fields as described in Ref. [34]. More information about the theoretical model and a summary of all parameters used for the simulation are given in Secs. S.2 and S.3 of the Supplemental Material [35]. The values for the g factor and $\alpha_{\mathrm{eff}}^{\mathrm{FMR}}$ are taken from the FMR experiments. M_{eff} and the total magnetic moment of the bilayer deviate slightly ($< 6\%$) from FMR and SQUID-VSM results. The SAW-SW coupling strength is described by $b_1^l \epsilon_{xx}^l/(|k||u_{z,0}^l|)$ and $b_{2,\mathrm{eff}}^l \epsilon_{xz}^l/(|k||u_{z,0}^l|)$,

which are obtained by curve fitting of the response of the magnetic single layers, as described in Ref. [12]. Here, $u_{z,0}^l$ is the amplitude of the lattice displacement in the z direction. Additional information about the simulation results, displayed in Fig. 3(d), is presented in Sec. S.3 of the Supplemental Material [35]. Simulation and experiment show excellent agreement with respect to all salient features such as resonance fields, nonreciprocity, linewidth, and transmission magnitude.

We further demonstrate this very good agreement for the resonance fields in Fig. 4(a) in more detail. Additionally, the simulated symmetry of the excited SW modes is given by the color code of the simulated resonance fields. First, the high- and low-field resonances have an inverted SW mode symmetry, which depends on ϕ_H. For low $|\phi_H|$ ($-16° \lesssim \phi_H \lesssim +13°$) the high-field resonance (low-frequency SW mode) has a symmetric SW mode shape, whereas the low-field resonance (high-frequency SW mode) has an antisymmetric SW mode shape. For increasing $|\phi_H|$ the magnitude of the effective interlayer dipolar coupling fields increases [34] and the SW mode symmetry changes. As described in the theory section, the symmetry of the SW mode influences the amplitude nonreciprocity, being induced by the SAW-SW helicity mismatch effect. For our magnetic bilayer, the effective coupling constants, $b_{2,\mathrm{eff}}^{\mathrm{Py}}$ and $b_{2,\mathrm{eff}}^{\mathrm{CoFeB}}$, have the same sign. Thus, for the antisymmetric (symmetric) SW mode, the first term in Eq. (3) partly cancels out (adds up) and the amplitude nonreciprocity is lowered (increased). This behavior is experimentally observed in Figs. 3(c) and 4(a) for high $|\phi_H|$ ($\phi_H \lesssim -16°, \phi_H \gtrsim 13°$). For lower $|\phi_H|$ this does not apply, because the interlayer coupling is weaker and mainly the CoFeB (Py) moments precess for the low (high) field SW resonance.

With reference to Fig. 4(b) we discuss the influence of the interlayer dipolar coupling strength on the position of the resonance fields by variation of the thickness of the Au spacer layer d_s. These simulations are carried out for Py(20)/Au(d_s)/CoFeB(5) with the parameters of the Py(20)/Au(5)/CoFeB(5) sample that are given in the Supplemental Material [35]. For a very large spacer layer thickness of $d_s = 10~\mu$m, the magnetic films are decoupled, such that the resonance fields are identical to the resonance fields of Py(20) and CoFeB(5) magnetic single layers. The resonance fields show an interception point at $\mu_0 H = 16$ mT. With decreasing spacer layer thickness the dipolar coupling strength increases. Thus, symmetric and antisymmetric SW modes form around 16 mT, which gives rise to anticrossing. Because the dipolar coupling strength increases with increasing $|\phi_H|$, also the induced shift of the resonance fields increases with $|\phi_H|$. For a small spacer layer thickness of $d_s = 5$ nm, the dipolar coupling is large and symmetric and antisymmetric SW modes form for all ϕ_H.
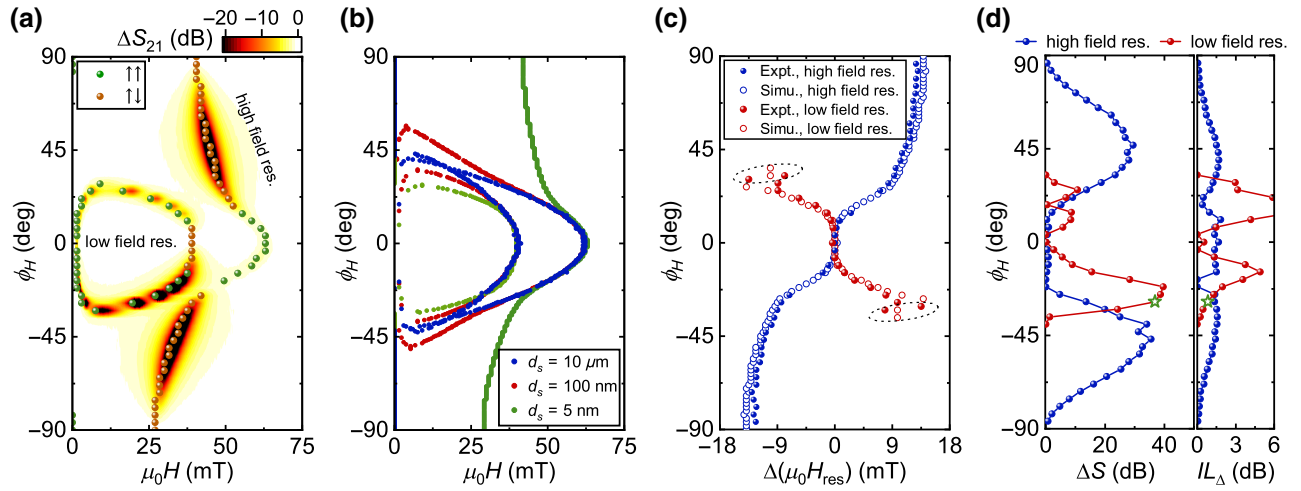
FIG. 4. (a) The resonance (res.) fields $\mu_0 H_{\text{res}}^{S21}$ of the experiment (false-color plot) and simulation (scatter plot) are in very good agreement. The symmetry of the simulated SW mode is given by the color of the simulated data points. (b) Simulated influence of the spacer layer thickness d_s on the resonance fields for Py(20)/Au(d_s)/CoFeB(5) magnetic bilayer films. The numbers in parentheses are the nominal film thicknesses in nanometers. (c) Nonreciprocal splitting of the resonance fields $\Delta(\mu_0 H_{\text{res}})$ for the low- and high-field resonance and for positive magnetic fields [see (a)]. For the points inside the dashed ellipses, no resonance is observed for either S_{21} or S_{12}, for which $\mu_0 H_{\text{res}} = 0$ is used. (d) Nonreciprocity of the transmission magnitude ΔS and insertion loss IL_Δ for positive resonance fields. For the low-field resonance a strong nonreciprocity of 37 dB and simultaneously low IL_Δ of 0.8 dB are observed (green stars).

We now focus on the nonreciprocity of the SW dispersion, which results in nonreciprocal splitting $\Delta(\mu_0 H_{\text{res}}) = \mu_0 H_{\text{res}}^{S21} - \mu_0 H_{\text{res}}^{S12}$ of the resonant fields H_{res}^{Sij}. The nonreciprocity $\Delta(\mu_0 H_{\text{res}})$ versus ϕ_H is shown in Fig. 4(c). Again, experiment and simulation agree well. The sign of $\Delta(\mu_0 H_{\text{res}})$ is inverted for the low-field resonance and for the high-field resonance. Except around $\phi_H = 0°$, $\Delta(\mu_0 H_{\text{res}})$ is approximately $\propto \sin\phi_H$, similar to the case of nonreciprocity induced by DMI [12,15,41], which is in agreement with the symmetry of the effective field of the interlayer coupling term that induces nonreciprocity [34].

For a wide range of angles ϕ_H the nonreciprocity $\Delta(\mu_0 H_{\text{res}})$ is large in comparison to the linewidth of the resonances and the resonances of ΔS_{21} and ΔS_{12} become separated. This is why we obtain in Fig. 4(d) a simultaneously large nonreciprocity of the transmission magnitude $\Delta S = |\Delta S_{21}(\mu_0 H_{\text{res}}^{S21}) - \Delta S_{12}(\mu_0 H_{\text{res}}^{S21})|$ and a low insertion loss $\text{IL}_\Delta = \text{Min} [|\Delta S_{21}(\mu_0 H_{\text{res}}^{S21})|, |\Delta S_{12}(\mu_0 H_{\text{res}}^{S21})|]$ at resonance $\mu_0 H_{\text{res}}^{S21}$. Note that we define the insertion loss IL_Δ as the insertion loss occurring by the resonant absorption of phonons in the magnetic field. Mainly due to the nonreciprocity of the SW dispersion, we observe around $\phi_H = \pm 45°$ a high nonreciprocity of about 32 dB and low IL_Δ of about 1.4 dB. Moreover, the nonreciprocity is additionally increased for the low-field resonance, because of the strong SAW-SW helicity mismatch effect. Thus, we obtain for $\phi_H = -28.8°$ both a large nonreciprocity of 37 dB and low IL_Δ of 0.8 dB for our 500-μm-long film sample. These values indicate that an acoustic isolator that is based on a dipolar-coupled magnetic bilayer is potentially more promising than approaches that solely

exploit the SAW-SW helicity mismatch effect [$\Delta S \approx 4.5$ dB/mm and $\text{IL}_\Delta \approx 5.0$ dB/mm for CoFeB(2) [12]] or approaches that are mainly based on DMI [$\Delta S \approx 27.9$ dB/mm and $\text{IL}_\Delta \approx 22.0$ dB/mm for CoFeB(5)/Pt(3) [12]].

In addition to the field-dependent insertion loss IL_Δ there is also the insertion loss IL_0 of the IDTs themselves being caused by the generation and detection of the acoustic waves. Our device consists of normal finger IDTs with three finger pairs. Therefore, it is optimized for SAW transmission measurements with high bandwidth, but has a high insertion loss of $\text{IL}_0 = -89$ dB for the measurements performed on the seventh harmonic resonance in Fig. 3. However, this insertion loss can be further optimized. It has been shown experimentally that an insertion loss as low as 6.2 dB (2.5 dB) can be realized at 4.1 GHz (2.0 GHz) by using floating-electrode-type unidirectional transducers [42,43].

For our magnetic bilayer sample, the nonreciprocal field shift $\Delta(\mu_0 H_{\text{res}})$ is large in comparison to the linewidth of the resonances. Therefore the resonances of ΔS_{21} and ΔS_{12} become separated, as discussed before. For samples that are not made from low-damping Py and CoFeB, it might be necessary to further increase $\Delta(\mu_0 H_{\text{res}})$, respectively the nonreciprocal splitting of the resonance frequencies $\Delta f_{\text{res}} = f_{\text{res}}(+k) - f_{\text{res}}(-k)$ [gray shaded areas for a constant $|k|$ in Fig. 2(c)] to obtain low IL_Δ.

The nonreciprocity can be improved in various ways. First, this can be achieved by increasing the magnetic film thicknesses. For moderate magnetic layer thicknesses ($d^l k \ll 1$), which are in a similar range ($d^l = d^A \approx d^B$), $\Delta f_{\text{res}} \propto d^l$, as shown in the Supplemental Material [35].

In comparison to interfacial DMI ($\Delta f_{res} \propto 1/d$ [44]), this behavior is of great advantage. With increasing d^l, not only does Δf_{res} increase, but additionally the SAW absorption ΔS_{ij}, which limits the maximum attainable nonreciprocity ΔS, increases. Moreover, the nonreciprocity in a dipolar-coupled bilayer does not rely on heavy metals. Thus, spin pumping [45], which results in a linewidth broadening $\propto 1/d$ for ΔS_{ij} [12], and a consequently increased IL_{Δ} are avoided.

Second, the interlayer dipolar fields decay exponentially with the thickness d_s of the spacer layer [34]. Therefore, thin spacers, such as $d_s = 5$ nm in our Py(20)/Au(5)/CoFeB(5) magnetic bilayer, are beneficial for resulting in a pronounced nonreciprocity. If d_s is further reduced, the nonreciprocity Δf_{res} is only slightly increased [<10% for Py(20)/Au(5)/CoFeB(5) at 7 GHz]. However, for very thin d_s interlayer exchange coupling may need to be considered.

Third, it is possible to maximize the nonreciprocity Δf_{res} by choosing magnetic films with an optimized ratio for the saturation magnetization M_s^l of both layers, as shown in the Supplemental Material [35]. Such an optimum exists, since the dipolar-coupling-induced nonreciprocity should be low for a magnetic bilayer made of (i) two almost identical layers [34] or (ii) one layer having a very low saturation magnetization.

While M_s^l, d_s, and d^l mainly determine the frequency nonreciprocity, the magnitude and sign of the respective magnetoelastic coupling constants and the type of SAW will impact the amplitude nonreciprocity due to the SAW-SW helicity mismatch effect.

Furthermore, the nonreciprocity Δf_{res} increases linearly with the wave vector k of the SW for $kd^l \ll 1$. This behavior is similar to that observed for DMI [44] and is tested by performing magnetoacoustic SW resonance measurements over a wide range of frequencies $0 < f < 7.5$ GHz and wave vectors $|k| = (2\pi f)/c_{SAW}$ ($0 < k < 15.1$ μm^{-1})

as a function of the external magnetic field [12]. The results are shown in Fig. 5 for $\phi_H = 9°, 21.6°$, and $81°$. Here, the relative change of the SAW transmission $\Delta S_{21}(f, \mu_0 H)$ is obtained by subtraction of the background offset $S_{21}(f, \mu_0 H = -200$ mT). With increasing ϕ_H the resonance frequency of the high-frequency branch strongly increases, whereas the resonance frequency of the low-frequency branch only slightly increases. As expected, the nonreciprocity, respectively the asymmetry of the resonant fields with respect to $H = 0$ clearly increases with ϕ_H and k and is inverted for the high- and low-frequency dispersion branches. The green points in Fig. 5 are the simulated resonance fields, obtained for the parameters given in Table SI of the Supplemental Material [35]. Again, we observe excellent agreement between experiment and simulation, which demonstrates that our model is adequate for describing the SAW-SW interaction over a wide range of frequencies and wave vectors. In addition, the two nonreciprocal SW resonance frequencies can be tuned by H and ϕ_H to approximately match two successive IDT resonance frequencies. Thereby, the two successive SAW transmission bands can have the same or inverted nonreciprocal behavior. This can be used to build a two-way unidirectional acoustic isolator [46,47], being based on MASW propagation.

V. ACOUSTIC ISOLATORS BASED ON DIPOLAR-COUPLED MAGNETIC BILAYERS

In the following, challenges in terms of building useful acoustic isolators are briefly discussed. First, the insertion loss of the acoustic isolator in the forward direction $IL_0 + IL_{\Delta}$ has to be low. The insertion loss of an optimized acoustic isolator is mainly given by the insertion loss IL_0 of the delay line out of SW resonance. SAW delay lines with an optimized insertion loss IL_0 of about -4 dB have been achieved in, for example, Refs. [42,43].
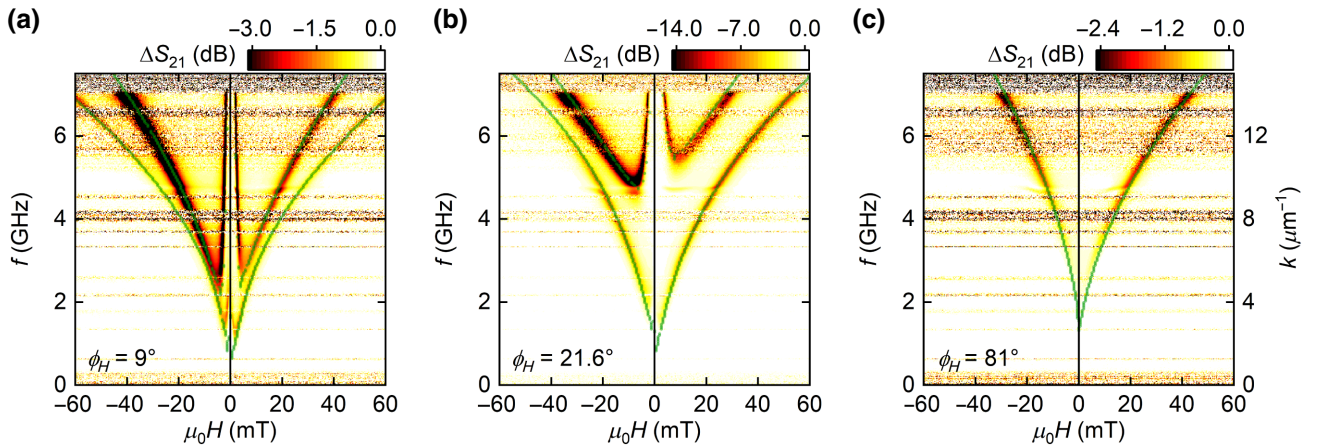

FIG. 5. Change of the experimentally determined SAW transmission ΔS_{21} as a function of the external magnetic field and frequency, respectively wave vector, for $\phi_H = 9°$ (a), $21.6°$ (b), and $81°$ (c). The green points indicate the simulation results.

Second, the nonreciprocity $\Delta S = |\Delta S_{21} - \Delta S_{12}|$ needs to be as large as possible. This is ideally achieved for high ΔS_{ij}, while $\Delta S_{ji} = 0$ ($IL_\Delta = 0$). In our device, a complete separation of the resonances of ΔS_{21} and ΔS_{12} is obtained for low effective damping constants $\alpha_{\mathrm{eff}}^{\mathrm{FMR}}$ of both investigated magnetic layers in conjunction with a high nonreciprocity of the SW dispersion. Additionally, the magnitude of the SAW absorption ΔS_{ij} is large, such that the prerequisites for the second condition are fulfilled in our experiments.

The nonreciprocity of the SW dispersion can be further increased by increasing the magnetic layer thicknesses, by choosing an optimized ratio for the saturation magnetization of both layers, or increasing the frequency. Furthermore, a drastic increase of the nonreciprocity is expected for interlayer dipolar- and exchange-coupled magnetic bilayers in antiferromagnetic alignment [34].

The magnitude of the SAW absorption ΔS_{ij} and thus the nonreciprocity ΔS can be in principle increased arbitrarily by increasing the length or the thickness of the magnetic films. However, long and thick magnetic films might increase unfavorable SAW propagation losses [48] and might consequently increase the insertion loss of the delay line IL_0. It is beyond the scope of our study to discuss such SAW propagation losses in more detail. Moreover, the magnitude of the SAW absorption ΔS_{ij} can be strongly increased by using magnetic films with a high magnetoelastic coupling constant b_1^l, since the magnitude of the magnetoelastic SAW-SW interaction ΔS_{ij} increases quadratically with b_1^l [35]. Promising highly magnetostrictive materials are Fe-Co-Si-B [49,50], Fe-Ga [51], Fe-Ga-B [22,52], and Tb-Dy-Fe [53]. However, since highly magnetostrictive materials usually come with increased SW damping [54], achieving low values for IL_Δ might be more challenging for these materials than for our low-damping Py(20)/Au(5)/CoFeB(5) magnetic bilayer.

VI. CONCLUSION

In conclusion, our experimental findings demonstrate the potential of nonreciprocal magnetoacoustic waves in a dipolar-coupled ferromagnetic bilayer for the realization of acoustic isolators. The employed Py(20)/Au(5)/CoFeB(5) sample shows at 6.87 GHz both a very large nonreciprocity of $\Delta S = 74$ dB/mm and a low insertion loss of $IL_\Delta = 1.6$ dB/mm, which is caused by SAW-SW interaction. Furthermore, the excellent agreement between theory and experiment demonstrates that MASW spectroscopy can be used to study SW modes of various magnetic multilayer systems.

We believe that SAW-SW coupling in magnetic bi- or multilayers has a high potential for characterizing SW dispersion, and interlayer coupling phenomena, as well as for a possible optimization of nonreciprocal effects, because

of the wide range of the tunability in magnetic thin-film systems.

First, the nonreciprocity in a dipolar-coupled magnetic bilayer can be easily increased by increasing the magnetic layer thicknesses or by choosing an optimized ratio for the saturation magnetization of both layers. Therefore, extremely high ΔS and low IL_Δ should be achievable for magnetic bilayers, being composed of high magnetostrictive materials. Moreover, in ultrathin magnetic films, DMI can be utilized to tune and strongly enhance the nonreciprocity, as theoretically predicted by Szulc *et al.* [31].

Finally, by choosing appropriate nonmagnetic spacer layers, interlayer exchange interactions can be leveraged to build synthetic antiferromagnets [55]. We expect that efficient SAW-driven SW excitation is enabled by the internal magnetoacoustic driving fields even in a synthetic antiferromagnet with zero net magnetization. This is in contrast to the small excitation efficiency by Oersted fields in such systems. On the one hand, the realization of a wide-band acoustic isolator was theoretically proposed in a synthetic antiferromagnet [3]. On the other hand, nonreciprocity in magnetic bilayers with antiparallel magnetization is larger than in magnetic bilayers with parallel magnetization [34]. Thus, switching the magnetization states by electrical currents via, for example, Oersted fields, spin-transfer, or spin-orbit torques might be a possible path towards reconfigurable acoustic isolators [34,56].

[1] A. A. Maznev, A. G. Every, and O. B. Wright, Reciprocity in reflection and transmission: What is a 'phonon diode'? Wave Motion **50**, 776 (2013).

[2] F. D. M. Haldane and S. Raghu, Possible Realization of Directional Optical Waveguides in Photonic Crystals with Broken Time-Reversal Symmetry, Phys. Rev. Lett. **100**, 013904 (2008).

[3] R. Verba, V. Tiberkevich, and A. Slavin, Wide-Band Nonreciprocity of Surface Acoustic Waves Induced by Magnetoelastic Coupling with a Synthetic Antiferromagnet, Phys. Rev. Appl. **12**, 054061 (2019).

[4] H. B. G. Casimir, On Onsager's principle of microscopic reversibility, Rev. Mod. Phys. **17**, 343 (1945).

[5] J. S. Lamb and J. A. Roberts, Time-reversal symmetry in dynamical systems: A survey, Physica D **112**, 1 (1998).

[6] M. Rotter, A. V. Kalameitsev, A. O. Govorov, W. Ruile, and A. Wixforth, Charge Conveyance and Nonlinear Acoustoelectric Phenomena for Intense Surface Acoustic Waves on a Semiconductor Quantum Well, Phys. Rev. Lett. **82**, 2171 (1999).

[7] M. Rotter, A. Wixforth, A. O. Govorov, W. Ruile, D. Bernklau, and H. Riechert, Nonlinear acoustoelectric interactions in GaAs/LiNbO₃ structures, Appl. Phys. Lett. **75,** 965 (1999).

[8] L. Dreher, M. Weiler, M. Pernpeintner, H. Huebl, R. Gross, M. S. Brandt, and S. T. B. Goennenwein, Surface acoustic wave driven ferromagnetic resonance in nickel thin films: Theory and experiment, Phys. Rev. B **86,** 134415 (2012).

[9] R. Sasaki, Y. Nii, Y. Iguchi, and Y. Onose, Nonreciprocal propagation of surface acoustic wave in Ni/LiNbO₃, Phys. Rev. B **95,** 020407(R) (2017).

[10] S. Tateno and Y. Nozaki, Highly Nonreciprocal Spin Waves Excited by Magnetoelastic Coupling in a Ni/Si Bilayer, Phys. Rev. Appl. **13,** 034074 (2020).

[11] M. Xu, K. Yamamoto, J. Puebla, K. Baumgaertl, B. Rana, K. Miura, H. Takahashi, D. Grundler, S. Maekawa, and Y. Otani, Nonreciprocal surface acoustic wave propagation via magneto-rotation coupling, Sci. Adv. **6,** eabb1724 (2020).

[12] M. Küß, M. Heigl, L. Flacke, A. Hörner, M. Weiler, M. Albrecht, and A. Wixforth, Nonreciprocal Dzyaloshinskii–Moriya Magnetoacoustic Waves, Phys. Rev. Lett. **125,** 217203 (2020).

[13] M. Küß, M. Heigl, L. Flacke, A. Hefele, A. Hörner, M. Weiler, M. Albrecht, and A. Wixforth, Symmetry of the Magnetoelastic Interaction of Rayleigh and Shear Horizontal Magnetoacoustic Waves in Nickel Thin Films on LiTaO₃, Phys. Rev. Appl. **15,** 034046 (2021).

[14] A. Hernández-Mínguez, F. Macià, J. M. Hernàndez, J. Herfort, and P. V. Santos, Large Nonreciprocal Propagation of Surface Acoustic Waves in Epitaxial Ferromagnetic/Semiconductor Hybrid Structures, Phys. Rev. Appl. **13,** 044018 (2020).

[15] D. Cortés-Ortuño and P. Landeros, Influence of the Dzyaloshinskii–Moriya interaction on the spin-wave spectra of thin films, J. Phys.: Condens. Matter **25,** 156001 (2013).

[16] J.-H. Moon, S.-M. Seo, K.-J. Lee, K.-W. Kim, J. Ryu, H.-W. Lee, R. D. McMichael, and M. D. Stiles, Spin-wave propagation in the presence of interfacial Dzyaloshinskii-Moriya interaction, Phys. Rev. B **88,** 184404 (2013).

[17] R. Zivieri, A. Giordano, R. Verba, B. Azzerboni, M. Carpentieri, A. N. Slavin, and G. Finocchio, Theory of nonreciprocal spin-wave excitations in spin hall oscillators with Dzyaloshinskii-Moriya interaction, Phys. Rev. B **97,** 134416 (2018).

[18] R. Verba, I. Lisenkov, I. Krivorotov, V. Tiberkevich, and A. Slavin, Nonreciprocal Surface Acoustic Waves in Multilayers with Magnetoelastic and Interfacial Dzyaloshinskii-Moriya Interactions, Phys. Rev. Appl. **9,** 064014 (2018).

[19] P. Grünberg, Some ways to modify the spin–wave mode spectra of magnetic multilayers, J. Appl. Phys. **57,** 3673 (1998).

[20] M. Vohl, J. Barnás, and P. Grünberg, Effect of interlayer exchange coupling on spin-wave spectra in magnetic double layers: Theory and experiment, Phys. Rev. B **39,** 12003 (1989).

[21] R. E. Camley and A. A. Maradudin, Magnetostatic interface waves in ferromagnets, Solid State Commun. **41,** 585 (1982).

[22] P. J. Shah, D. A. Bas, I. Lisenkov, A. Matyushov, N. X. Sun, and M. R. Page, Giant nonreciprocity of surface acoustic waves enabled by the magnetoelastic interaction, Sci. Adv. **6,** eabc5648 (2020).

[23] H. Bömmel and K. Dransfeld, Excitation of Hypersonic Waves by Ferromagnetic Resonance, Phys. Rev. Lett. **3,** 83 (1959).

[24] M. Weiler, L. Dreher, C. Heeg, H. Huebl, R. Gross, M. S. Brandt, and S. T. B. Goennenwein, Elastically Driven Ferromagnetic Resonance in Nickel Thin Films, Phys. Rev. Lett. **106,** 117601 (2011).

[25] S. Maekawa and M. Tachiki, Surface acoustic attenuation due to surface spin wave in ferro- and antiferromagnets, AIP Conf. Proc. **29,** 542 (1976).

[26] M. Matsuo, J. Ieda, E. Saitoh, and S. Maekawa, Effects of Mechanical Rotation on Spin Currents, Phys. Rev. Lett. **106,** 076601 (2011).

[27] M. Matsuo, J. Ieda, K. Harii, E. Saitoh, and S. Maekawa, Mechanical generation of spin current by spin-rotation coupling, Phys. Rev. B **87,** 180402(R) (2013).

[28] D. Kobayashi, T. Yoshikawa, M. Matsuo, R. Iguchi, S. Maekawa, E. Saitoh, and Y. Nozaki, Spin Current Generation Using a Surface Acoustic Wave Generated via Spin-Rotation Coupling, Phys. Rev. Lett. **119,** 077202 (2017).

[29] Y. Kurimune, M. Matsuo, and Y. Nozaki, Observation of Gyromagnetic Spin Wave Resonance in NiFe Films, Phys. Rev. Lett. **124,** 217205 (2020).

[30] P. Grünberg, Magnetostatic spinwave modes of a ferromagnetic double layer, J. Appl. Phys. **51,** 4338 (1980).

[31] K. Szulc, P. Graczyk, M. Mruczkiewicz, G. Gubbiotti, and M. Krawczyk, Spin-Wave Diode and Circulator Based on Unidirectional Coupling, Phys. Rev. Appl. **14,** 034063 (2020).

[32] P. Grünberg, J. Barnas, F. Saurenbach, J. Fuß, A. Wolf, and M. Vohl, Layered magnetic structures: Antiferromagnetic type interlayer coupling and magnetoresistance due to antiparallel alignment, J. Magn. Magn. Mater. **93,** 58 (1991).

[33] A. Fuß, S. Demokritov, P. Grünberg, and W. Zinn, Short- and long period oscillations in the exchange coupling of Fe across epitaxially grown Al- and Au-interlayers, J. Magn. Magn. Mater. **103,** L221 (1992).

[34] R. A. Gallardo, T. Schneider, A. K. Chaurasiya, A. Oelschlägel, S. S. P. K. Arekapudi, A. Roldán-Molina, R. Hübner, K. Lenz, A. Barman, J. Fassbender, J. Lindner, O. Hellwig, and P. Landeros, Reconfigurable Spin-Wave Nonreciprocity Induced by Dipolar Interaction in a Coupled Ferromagnetic Bilayer, Phys. Rev. Appl. **12,** 034012 (2019).

[35] See Supplemental Material at http://link.aps.org/supplemental/10.1103/PhysRevApplied.15.034060 for details about the sample preparation [S.1], the theoretical model [S.2], additional curve fitting results and the summary Table SI [S.3], and tuning the nonreciprocity of a magnetic bilayer [S.4], which includes Refs. [8,11–13,15,26–29,34,40,44, 45,48,57–64].

[36] B. Heinrich, Y. Tserkovnyak, G. Woltersdorf, A. Brataas, R. Urban, and G. E. W. Bauer, Dynamic Exchange Coupling in Magnetic Bilayers, Phys. Rev. Lett. **90,** 187601 (2003).

[37] S. Klingler, V. Amin, S. Geprägs, K. Ganzhorn, H. Maier-Flaig, M. Althammer, H. Huebl, R. Gross, R. D. McMichael, M. D. Stiles, S. T. B. Goennenwein, and M. Weiler, Spin-Torque Excitation of Perpendicular Standing Spin Waves in Coupled YIG/Co Heterostructures, Phys. Rev. Lett. **120,** 127201 (2018).

[38] M. Hiebel, *Grundlagen der Vektoriellen Netzwerkanalyse* (Rohde & Schwarz, München, 2011), 3rd ed.

[39] D. Labanowski, A. Jung, and S. Salahuddin, Power absorption in acoustically driven ferromagnetic resonance, Appl. Phys. Lett. **108,** 022905 (2016).

[40] E. Klokholm and J. A. Aboaf, The saturation magnetostriction of permalloy films, J. Appl. Phys. **52,** 2474 (1981).

[41] V. L. Zhang, K. Di, H. S. Lim, S. C. Ng, M. H. Kuok, J. Yu, J. Yoon, X. Qiu, and H. Yang, In-plane angular dependence of the spin-wave nonreciprocity of an ultrathin film with Dzyaloshinskii-Moriya interaction, Appl. Phys. Lett. **107,** 022402 (2015).

[42] K. Yamanouchi, C. Lee, K. Yamamoto, T. Meguro, and H. Odagawa, in *IEEE 1992 Ultrason. Symposium*, edited by B. R. McAvoy (IEEE, New York, 1992) p. 139.

[43] M. K. Ekström, T. Aref, J. Runeson, J. Björck, I. Boström, and P. Delsing, Surface acoustic wave unidirectional transducers for quantum applications, Appl. Phys. Lett. **110,** 073105 (2017).

[44] H. T. Nembach, J. M. Shaw, M. Weiler, E. Jué, and T. J. Silva, Linear relation between Heisenberg exchange and interfacial Dzyaloshinskii–Moriya interaction in metal films, Nat. Phys. **11,** 825 (2015).

[45] Y. Tserkovnyak, A. Brataas, and G. E. W. Bauer, Enhanced Gilbert Damping in Thin Ferromagnetic Films, Phys. Rev. Lett. **88,** 117601 (2002).

[46] Y. Chen, Y. Huang, C. Lü, and W. Chen, A two-way unidirectional narrow-band acoustic filter realized by a graded phononic crystal, J. Appl. Mech. **84,** 091003 (2017).

[47] Y. Chen, B. Wu, Y. Su, and W. Chen, Tunable two-way unidirectional acoustic diodes: Design and simulation, J. Appl. Mech. **86,** 031010 (2019).

[48] D. P. Morgan, *Surface Acoustic Wave Filters: With Applications to Electronic Communications and Signal Processing* (Elsevier, Amsterdam, 2007), 2nd ed.

[49] K.-H. Shin, M. Inoue, and K.-I. Arai, Elastically coupled magneto-electric elements with highly magnetostrictive amorphous films and PZT substrates, Smart Mater. Struct. **9,** 357 (2000).

[50] A. Kittmann, P. Durdaut, S. Zabel, J. Reermann, J. Schmalz, Be. Spetzler, D. Meyners, N. X. Sun, J. McCord, M. Gerken, G. Schmidt, M. Höft, R. Knöchel, F. Faupel, and E. Quandt, Wide band low noise Love wave magnetic field sensor system, Sci. Rep. **8,** 1 (2018).

[51] D. E. Parkes, L. R. Shelford, P. Wadley, V. Holý, M. Wang, A. T. Hindmarch, G. van der Laan, R. P. Campion, K. W. Edmonds, S. A. Cavill, and A. W. Rushforth, Magnetostrictive thin films for microwave spintronics, Sci. Rep. **3,** 2220 (2013).

[52] J. Lou, R. E. Insignares, Z. Cai, K. S. Ziemer, M. Liu, and N. X. Sun, Soft magnetism, magnetostriction, and microwave properties of FeGaB thin films, Appl. Phys. Lett. **91,** 182504 (2007).

[53] R. C. O'Handley, *Modern Magnetic Materials: Principles and Applications* (Wiley, New York, NY, 1999).

[54] P. G. Gowtham, G. E. Rowlands, and R. A. Buhrman, A critical analysis of the feasibility of pure strain-actuated giant magnetostrictive nanoscale memories, J. Appl. Phys. **118,** 183903 (2015).

[55] R. A. Duine, Kyung-Jin Lee, Stuart S. P. Parkin, and M. D. Stiles, Synthetic antiferromagnetic spintronics, Nat. Phys. **14,** 217 (2018).

[56] M. Ishibashi, Y. Shiota, T. Li, S. Funada, T. Moriyama, and T. Ono, Switchable giant nonreciprocal frequency shift of propagating spin waves in synthetic antiferromagnets, Sci. Adv. **6,** eaaz6931 (2020).

[57] C. Tannous and J. Gieraltowski, The Stoner–Wohlfarth model of ferromagnetism, Eur. J. Phys. **29,** 475 (2008).

[58] W. P. Robbins, A simple method of approximating surface acoustic wave power densities, IEEE Trans. Son. Ultrason. **24,** 339 (1977).

[59] B. A. Kalinikos and A. N. Slavin, Theory of dipole-exchange spin wave spectrum for ferromagnetic films with mixed exchange boundary conditions, J. Phys. C: Solid State Phys. **19,** 7013 (1986).

[60] H. Yang, A. Thiaville, S. Rohart, A. Fert, and M. Chshiev, Anatomy of Dzyaloshinskii-Moriya Interaction at Co/Pt Interfaces, Phys. Rev. Lett. **115,** 267210 (2015).

[61] COMSOL Multiphysics® v. 5.4. www.comsol.com. COMSOL AB, Stockholm, Sweden.

[62] J. Cho, J. Jung, K.-E. Kim, S.-I. Kim, S.-Y. Park, M.-H. Jung, and You Chun-Yeol, Effects of sputtering Ar gas pressure in the exchange stiffness constant of $Co_{40}Fe_{40}B_{20}$ thin films, J. Magn. Magn. Mater. **339,** 36 (2013).

[63] E. Blackburn, C. Sanchez-Hanke, S. Roy, D. J. Smith, J.-I. Hong, K. T. Chan, A. E. Berkowitz, and S. K. Sinha, Pinned Co moments in a polycrystalline permalloy/CoO exchange-biased bilayer, Phys. Rev. B **78,** 180408(R) (2008).

[64] J. M. Barandiarán, J. Gutiérrez, Z. Kaczkowski, and D. de Cos, Influence of annealing temperature on the magnetic and magnetoelastic properties in Fe–Co–B metallic glasses, J. Non-Cryst. Solids **329,** 43 (2003).